Supplementary Information

Formation of mixed-phase $Ni_xB/Co_3O_4/Co(OH)_2$ and its application as a pre-catalyst for the oxygen evolution reaction

Gillian Collins[1], Ramaraj Sukanya[1], Daniele Alves[1], Thamaraiselvi Kanagaraj[2], Raj Karthik[1], Tara N Barwa[1], Jae-Jin Shim[2], and Carmel B. Breslin[1,3*]

[1]Department of Chemistry, Maynooth University, Maynooth, Co. Kildare, Ireland

[2]School of Chemical Engineering, Yeungnam University, 280 Daehak-ro, Gyeongsan, Gyeongbuk 38541, Republic of Korea.

[3]Kathleen Lonsdale Institute, Maynooth University, Maynooth, Co. Kildare, Ireland

*Corresponding author, Carmel.Breslin@mu.ie

Chemical and Materials

All chemicals were purchased in analytical grade and used without further purification. Nickel (II) chloride hexahydrate ($NiCl_2.6H_2O$, 99.3%), Cobalt (II) chloride hexahydrate ($CoCl_2.6H_2O$, 97%), Urea (NH_2CONH_2, 99%), Hexadecyltrimethylammonium bromide ($CH_3(CH_2)15N(Br)(CH_3)_3$, >98%), sodium hydroxide (NaOH), potassium hydroxide pellets (KOH, 85%), polyvinylidene fluoride (PVDF), carbon black (99.9%), ethanol (C_2H_5OH, 99.5%), 1-methyl-2-pyrrolidone (NMP, 99.5%), hydrochloric acid (HCl, 35-37%) and sodium borohydride ($NaBH_4$, 98%) were purchased from Sigma Aldrich. Carbon cloth (CC) was cut from a carbon cloth roll (1071 HCB) purchased from Fuel Cell Earth LLC. Nickel Foam (NF) was cut from a nickel foam roll (1000 mm x 300 mm x 1.6 mm) purchased from Nano Graphi. Nickel foam pieces were then cut to size and pressed to approximately 0.1 mm. All solutions and reagents required for this work were prepared with deionised water (DI).

Materials Characterization

The composite was characterised using a combination of techniques, including SEM, XRD, Raman spectroscopy and XPS. Morphological analysis was conducted using a Hitachi S-4800 field emission scanning electron microscope (FE-SEM). Information about the crystallinity of the composites was obtained via powder X-ray diffraction (PXRD) on a PANalytical X'Pert PRO MPD system. Raman spectra were collected using a Horiba XploRA PLUS Raman spectrometer with a 532 nm excitation source to identify vibrational features of the material. Surface composition and oxidation states, both before and after electrochemical testing in 1.0 M KOH, were examined using X-ray photoelectron spectroscopy (XPS) on a Kratos AXIS ULTRA system.

Electrochemical Measurements

Electrochemical analyses were conducted using a three-electrode configuration. The catalyst loading on the electrode was maintained at approximately 0.4 mg cm^{-2}. Cyclic voltammetry (CV), linear sweep voltammetry (LSV), and chronoamperometry were performed to examine the catalytic activity of the materials for OER in 1 M KOH. Electrochemical measurements were performed using a Solartron SI-1287 electrochemical workstation with a three-electrode system and a 1.0 M KOH electrolyte solution. The modified CC/NF, high surface area platinum wire, and a Hg/HgO electrode were employed as the working, counter, and reference electrodes, respectively. The electrode potentials were converted to the reversible hydrogen electrode (RHE) scale using the relationship,

$E_{RHE} = E_{Hg/HgO} + 0.098 + 0.0592\ pH.$

Linear sweep voltammetry (LSV) was acquired at a scan rate of 2 mV s^{-1}. For Tafel analysis, current densities were sampled from the steady-state region of chronoamperometric responses to construct the Tafel plot equation, where η is the overpotential, j is the measured current density, b is the Tafel slope and a is a constant containing the exchange current density, j_o.

$$\eta = a + b \log |j| \quad (1)$$

Electrochemical impedance spectroscopy (EIS) was used to measure the charge transfer resistance (R_{ct}) values over a frequency range of 100 kHz to 0.1 Hz, in the non-faradic region, typically around 0.05 V vs Hg/HgO. Chronopotentiometry was employed to evaluate the stability of the catalyst for OER performance at a catalytic turnover potential of 1.6 V vs. RHE in 1.0 M KOH.

Schemes, Figures and Tables

Table S1: Influence of Ni_xB/CoO-100 loading onto CC and its influence on the overpotential of the OER at current densities of 10 and 50 mA cm^{-2}

Mass loading (mg cm^{-2})	η_{10} (mV)	η_{50} (mV)
0.2	333	470
0.3	327	426
0.4	330	410
0.5	343	429
0.6	371	490

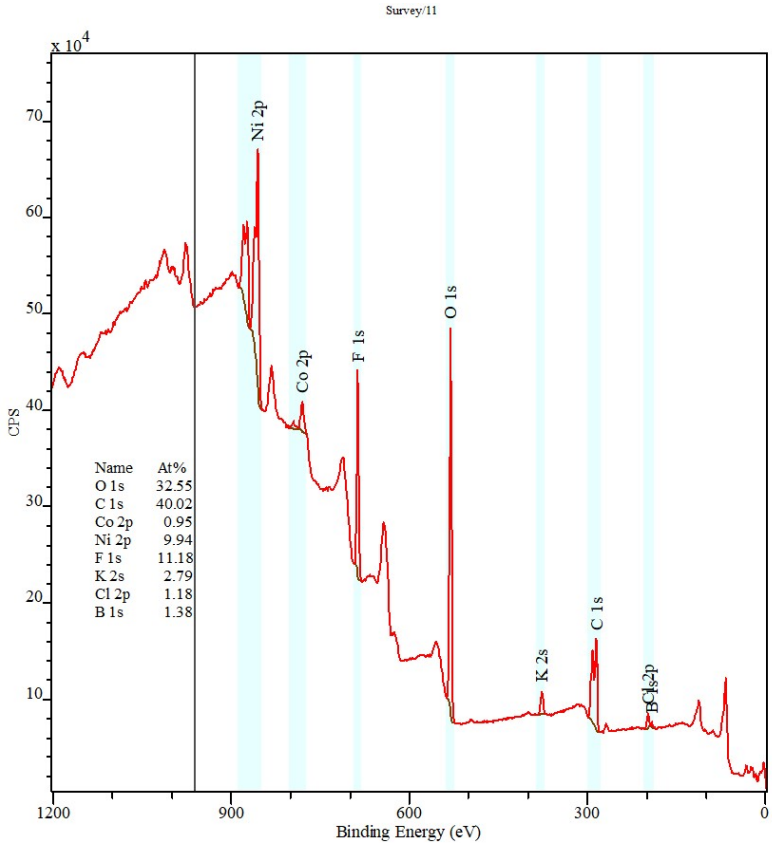

Figure S1: Survey spectrum for Ni_xB/CoO-100 composite.

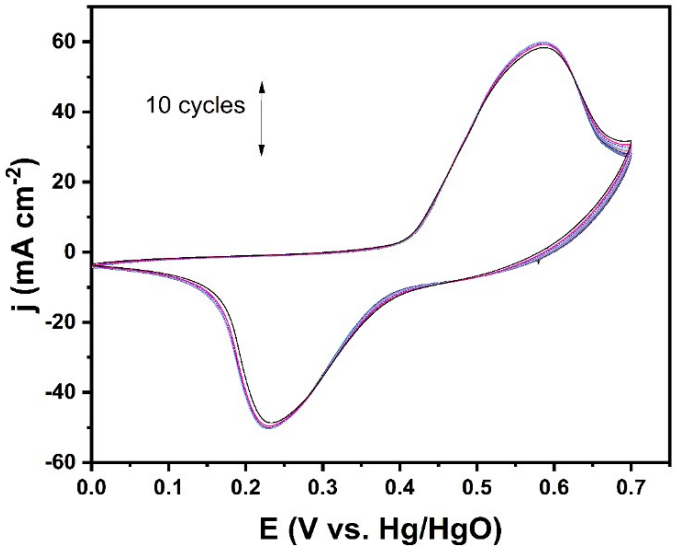

Figure S2: CV activation cycling of Ni_xB/CoO-100@CC from 0 V and 0.7 V (vs Hg/HgO) at a scan rate of 50 mV/s in 1.0 M KOH.

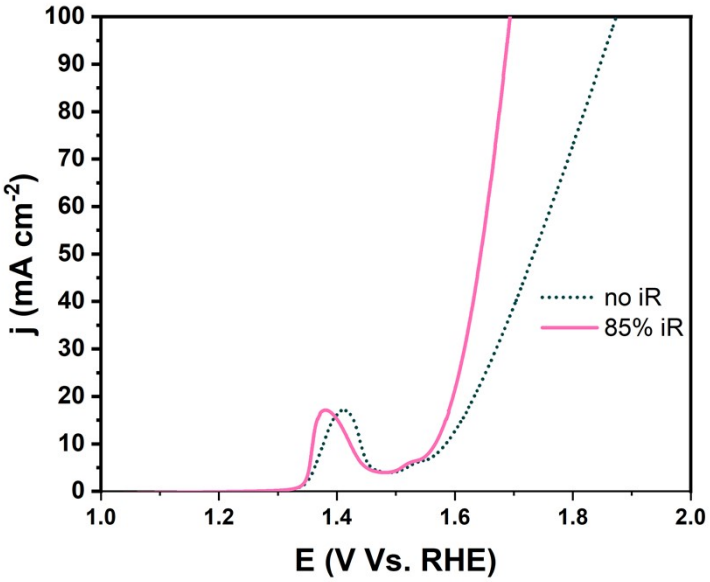

Figure S3: Influence of IR correction, comparing the recorded data with the 85% IR corrected data.

Table S2: Summary of ECSA analysis

Sample	C_{dl} (µF)	ECSA (cm^2 mg^{-1})	ECSA Ratio to CC
CC	194.74	4.87	1
Ni_xB/CoO-100@CC	3913.5	97.84	20.1
NiXb@CC	1217.6	30.44	6.25
Co_3O_4@CC	2383.6	59.59	12.24

*The CPE-T value (obtained from EIS in the non-faradic region) of CC (containing carbon black and PVDF binder but no active catalyst) provides a relative ratio of 3913.5/194.74 = 20.1 for Ni_xB/CoO-100@CC composite relative to the CC.

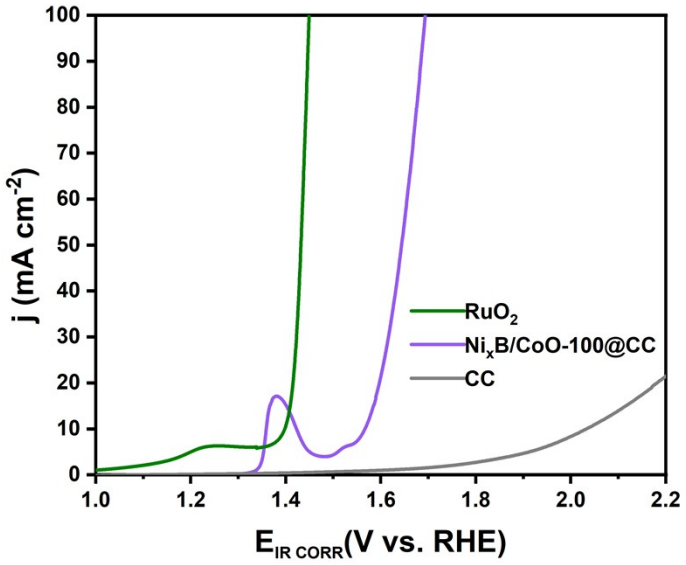

Figure S4: LSV curves recorded for RuO_2, Ni_xB/CoO-100@CC and CC in KOH.

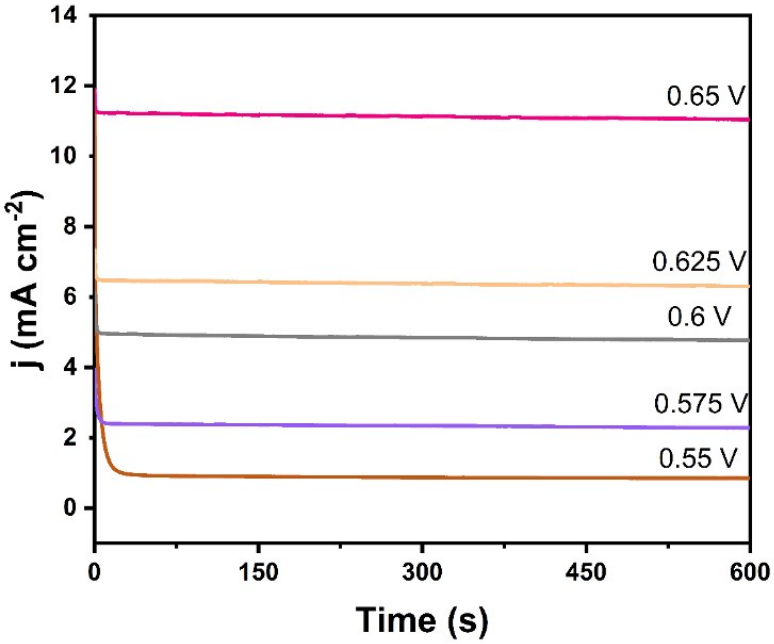

Figure S5: Chronoamperometry data recorded for the estimation of the Tafel slopes for Ni_xB/CoO-100@CC in 1.0 M KOH with the potentials shown on the Hg/HgO scale.

.

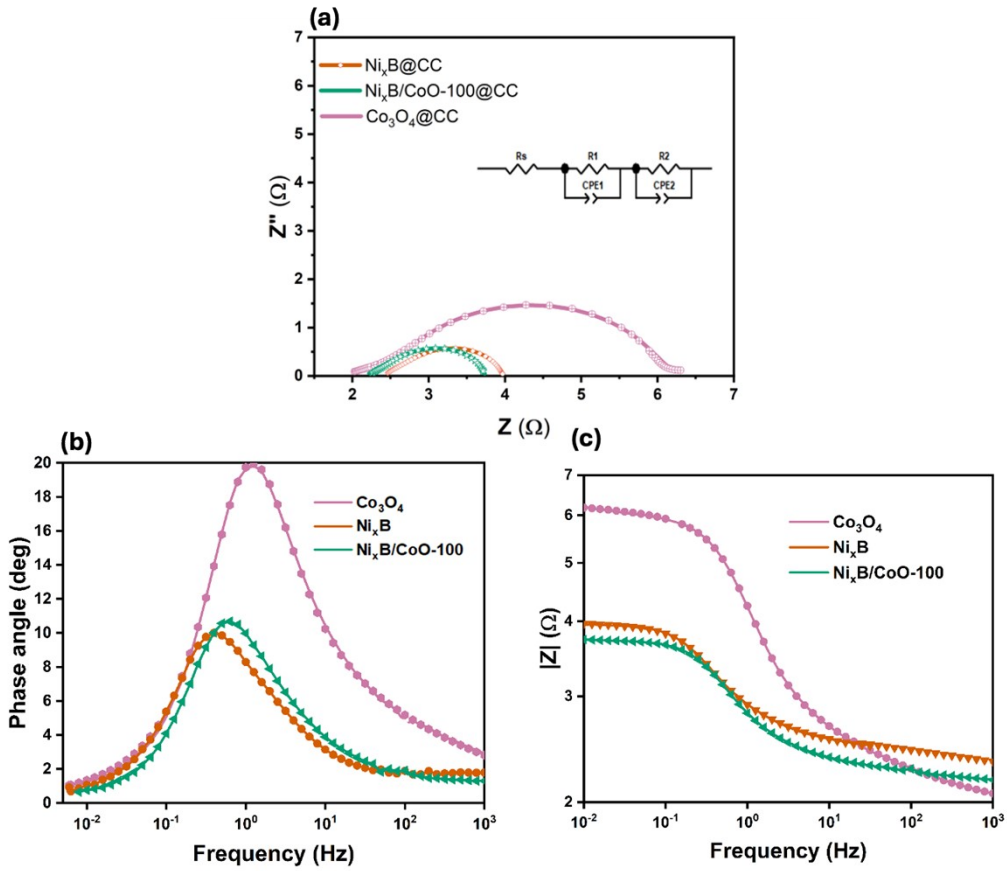

Figure S6: Nyquist and Bode plots recorded for Ni_xBCoO-100 and its individual components supported on CC recorded during the OER.

Table S3: Summary of the equivalent circuit parameters.

	Co_3O_4@CC	**Ni_xB@CC**	**Ni_xB/CoO-100@CC**
R1 (Ω)	1.84 ± 0.05	0.80 ± 0.06	0.58 ± 0.04
CPE1-T ($\Omega^{-1}s^n$)	0.18 ± 0.00	0.41 ± 0.01	0.35 ± 0.02
CPE1-P	0.37 ± 0.01	0.61 ± 0.01	0.59 ± 0.01
R2 (Ω)	2.63 ± 0.04	0.77 ± 0.06	0.95 ± 0.04
CPE2-T ($\Omega^{-1}s^n$)	0.09 ± 0.00	0.69 ± 0.05	0.37 ± 0.01
CPE2-P	0.95 ± 0.01	1.02 ± 0.02	0.98 ± 0.01
R_{Total} (Ω)	4.47	1.57	1.53

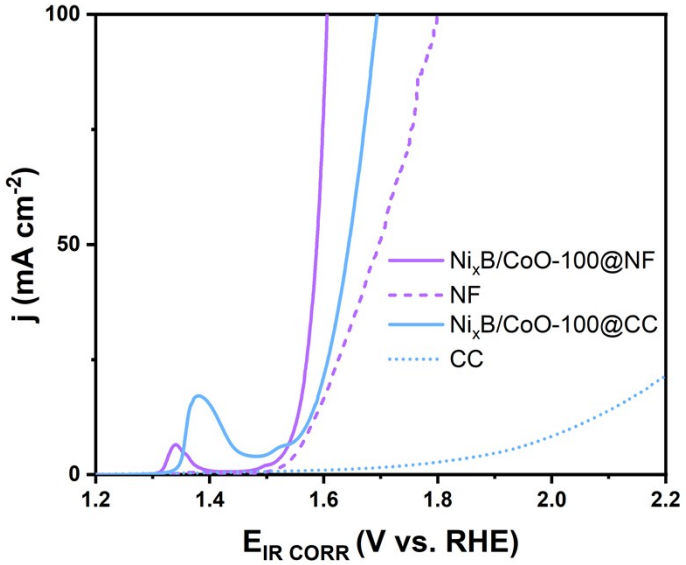

Figure S7: LSVs comparing the Ni_xB/CoO-100NF@NF, Ni_xB/CoO-100NF@CC, CC and NF.

Table S4: Comparison of Ni_xB/CoO-100@NF with recently reported OER electrocatalysts.

Catalyst	j (mA cm^{-2})	η (mV)	Stability (h)	Reference
RuO_2@NF	10	310	-	This work
	50	368		
	100	410		
Ni_xB/CoO-100@NF	10	316	94	
	50	354		
	100	370		
$Co_{1.5}Ni_3Fe_3$-LDH/G	10	350	72	1
	50	430		
B@NiO	10	191	17.5	2
	50	420		
Ti-NiCo-LDH/NF	50	319	150	3
	100	353		
NiCo-LDH/NF	50	391	-	
	100	429		
Cr-FeNi LDH/SS	10 100	280 420	20	4
NiCoCe-LDH/RNF	50	299	6	5
NiCo-LDH/NF	50	491	-	
CuCrFeNiCoP HEA	100	423	24	6
CuNiCo@CNT-2/NF	50	280	50	7
	100	350		
Co/Ni-MOF	100	410	8	8
$Ni_{50}Co_{50}P$/FS	10	400	-	9
	100	498		
$Ni_{30}Co_{70}$/NF	10	365	-	
	100	446		
NiO-B-$_X$	10	380	10	10
$CoMoO_4$	10	366	80	11
Co_2CrO_4/RuO_2	10	209	50	12
Co_3Fe_7/Fe_3O_4	10	279	12	13
$Ni_{2.5}B$@NF	10	279	10	14
FeCoNiMgB	10	268	72	15

References

(1) Alves, D.; Collins, G.; Dalla Benetta, M. B.; Dempsey, E.; Shim, J. J.; Karthik, R.; Breslin, C. B. Factorial Design and Optimization of Trimetallic CoNiFe-LDH/Graphene Composites for Enhanced Oxygen Evolution Reaction. *ACS Appl. Energy Mater.* **2025**, *8* (8). https://doi.org/10.1021/acsaem.5c00483.

(2) Wenelska, K.; Dymerska, A.; Mijowska, E. Promotion of Borophene/NiO-Based Electrocatalyst for Oxygen Evolution Reaction. *Chemical Engineering Journal* **2023**, *476*. https://doi.org/10.1016/j.cej.2023.146714.

(3) Xie, J.; Du, J.; Chen, P.; Wang, G.; Zhang, J.; Yang, X.; Kong, A.; Yu, F. A Facile Route of Ti Decoration for Modulating M–O–Ti (M = Ni, Co) and Oxygen Vacancies on NiCo-LDH Electrocatalysts for Efficient Oxygen Evolution Reaction. *Industrial Chemistry & Materials* **2025**, *3* (3). https://doi.org/10.1039/d5im00007f.

(4) Lv, Y.; Deng, X.; Ding, J.; Zhou, Y. In-Situ Fabrication of Cr Doped FeNi LDH on Commercial Stainless Steel for Oxygen Evolution Reaction. *Sci. Rep.* **2024**, *14* (1). https://doi.org/10.1038/s41598-023-50361-4.

(5) Qi, R.; Zhong, Z.; Jia, Y.; Chen, F.; Yang, Y.; Zheng, X.; Li, Q.; Ye, Q.; Du, H. Ce-Doped NiCo-Layered Double Hydroxide Based Self-Supporting Tremella-Shaped Nanoflower Heterostructure as Efficient Electrocatalyst for the Oxygen Evolution Reaction. *J. Environ. Chem. Eng.* **2024**, *12* (6). https://doi.org/10.1016/j.jece.2024.114376.

(6) Zhang, T.; Li, J.; Zhang, B.; Wang, G.; Jiang, K.; Zheng, Z.; Shen, J. High-Entropy Alloy CuCrFeNiCoP Film of Cu-Based as High-Efficiency Electrocatalyst for Water Splitting. *J. Alloys Compd.* **2023**, *969*. https://doi.org/10.1016/j.jallcom.2023.172439.

(7) Kumaravel, S.; Chandramoorthy, C.; Gnanasekaran, L.; Durai, M.; Vijayakumar, P.; Durai, M.; Priya, S.; Fatehmulla, A.; Alagarasan, J. K.; Ahn, Y. H. Multi-Walled Carbon Nanotube Integrated Ni–Co Hydroxide/Cu2(OH)3NO3 Heterostructures for Efficient Oxygen Evolution in Alkaline Media. *Electrochim. Acta* **2025**. https://doi.org/10.1016/j.electacta.2025.147859.

(8) Zhang, H.; Zhang, M.; Geng, Q.; Gao, X. Co/Ni-MOF as a Bifunctional Electrode Material for Electrochemical Sensor and Oxygen Evolution Reaction. *Mater. Lett.* **2024**, *355*. https://doi.org/10.1016/j.matlet.2023.135538.

(9) Parvanova-Mancheva, T.; Chakarova, V.; Gabrovska, M.; Atanasova - Vladimirova, S.; Baeva, A.; Andreeva, R.; Hodzhaoglu, F.; Nikolova, D. Evaluating the Bifunctional Properties towards HER and OER of NiCo Electrodeposited Coatings: Combined Influence of Support, Ni/Co Ratio, and Phosphorus Doping. *Catal. Today* **2025**, *460*. https://doi.org/10.1016/j.cattod.2025.115495.

(10) Idris, M. B.; Mamba, B. B.; Xolile, F. Facile Synthesis of Nickel Oxide/Delaminated Boron Composite with an Enhanced Electrocatalytic Activity Towards the Oxygen Evolution Reaction in Alkaline Medium. *Electrocatalysis* **2025**, *16* (6). https://doi.org/10.1007/s12678-025-00979-x.

(11) Zhong, X.; Chen, Y.; Gan, T.; Huang, Y.; Li, J.; Zhang, S. Unveiling the Superior Oxygen Evolution Reaction Performance of β-CoMoO4 Nanorods: Insights into Catalytic Mechanisms and Active Site Dynamics. *Nano Res.* **2025**, *18* (3). https://doi.org/10.26599/NR.2025.94907204.

(12) Qi, M.; Zheng, X.; Tong, H.; Liu, Y.; Li, D.; Yan, Z.; Jiang, D. Synergizing Ruthenium Oxide with Bimetallic Co2CrO4 for Highly Efficient Oxygen Evolution Reaction. *J. Colloid Interface Sci.* **2025**, *677*. https://doi.org/10.1016/j.jcis.2024.07.260.

(13) Barath, R.; Vadivel, S.; Sarmila, S.; Sujita, P.; Murugan, N.; Kim, Y. A. Core-Shell Co3Fe7/Fe3O4 Electrocatalyst via MOF Engineering: Unlocking Superior Oxygen Evolution Activity for Water Splitting. *Mater. Lett.* **2025**, *399*. https://doi.org/10.1016/j.matlet.2025.139056.

(14) Du, Y.; He, X.; Yan, C.; Hu, Q.; Zhang, J.; Yang, F. Promoted Surface Reconstruction of Amorphous Nickel Boride Electrocatalysts by Boron Dissolution for Boosting the Oxygen Evolution Reaction. *J. Mater. Chem. A Mater.* **2025**, *13* (11). https://doi.org/10.1039/d4ta08295h.

(15) Miao, F.; Cui, P.; Jing, Z.; Wu, W.; Zhang, Z.; Gu, T.; Yan, Z.; Liang, X. FeCoNiMgB High-Entropy Boride Powder with a Fluffy Cotton Structure and Enhanced Activity in the Oxygen Evolution Reaction. *Journal of Materials Research and Technology* **2024**, *30*. https://doi.org/10.1016/j.jmrt.2024.03.158.